MSFC-262

# First X-ray Observations Of The Young Pulsar J1357–6429

Vyacheslav E. Zavlin

*Space Science ~~Laboratory~~ Office, NASA MSFC ~~SD59~~ VP62, Huntsville, AL 35805;*
*vyacheslav.zavlin@msfc.nasa.gov*

## ABSTRACT

The first short *Chandra* and *XMM*-Newton observations of the young and energetic pulsar J1357–6429 provided strong indications of a tail-like pulsar-wind nebula associated with this object, as well as strong pulsations of its X-ray flux with a pulsed fraction above 40% and a thermal component dominating at lower photon energies (below 2 keV). The elongated nebular is very compact in size, about $1'' \times 1''.5$, and might be interpreted as a pulsar jet. The thermal radiation is most plausibly emitted from the entire neutron star surface of an effective temperature about 1 MK covered with a magnetized hydrogen atmosphere. At higher energies the pulsar's emission is of a nonthermal (magnetospheric) origin, with a power-law spectrum of a photon index $\Gamma \approx 1.1$. This makes the X-ray properties of PSR J1357–6429 very similar to those of the youngest pulsars J1119–6127 and Vela with a detected thermal radiation.

*Subject headings:* pulsars: individual (PSR J1357–6229) – stars: neutron — stars: X-rays

## 1. Introduction

Once discovered in radio, young rotation-powered pulsars (with characteristic ages of $\tau_c = P/2\dot{P} \sim 10$ kyr, where $P$ and $\dot{P}$ are pulsar spin period and its derivative) often become targets for X-ray observations. The reasons for this are rather straightforward: these objects usually possess large values of the rotational-energy loss, $\dot{E} = 4\pi^2 I \dot{P} P^{-3} \sim 10^{36}$–$10^{38}$ ergs s$^{-1}$ ($I \simeq 10^{45}$ g cm$^2$ is the moment of inertia of a neutron star [NS]), and are expected to generate observable nonthermal (magnetospheric) emission and power pulsar-wind nebulae (PWNe) detectable at different energies (see Kargaltsev, Pavlov, & Garmire 2007 for a compilation of properties of X-ray PWNe generated by a number of young pulsars). Measuring luminosities, spectra, and angular distribution of the magnetospheric radiation is particularly important for inferring emission processes operating in pulsar magnetosphere

and distinguishing between the two competing approaches, polar-cap and outer-gap models (e. g., Harding & Muslimov 2005; Zhang & Jiang 2006). Studying the spectrum and morphology of a PWN is essential for determining the energy of the pulsar wind, probing the ambient medium, and understanding the shock acceleration mechanism(s). On the other hand, NSs are born very hot in supernova explosions and cool down via neutrino emission from the entire NS body and heat transport through the stellar envelope to the surface and subsequent thermal surface emission of photons. The rate at which a NS cools down is mainly determined by various processes of the neutrino emission, as well as the (unknown) properties of the matter in the NS interior (see Yakovlev et al. 2005 for a review on the NS cooling). Till recently, it was generally thought that young pulsars are so powerful nonthermal X-ray emitters that thermal radiation from the stellar surface would be completely buried under the nonthermal component, making it virtually impossible to accurately measure the thermal flux: only upper limits on the surface temperature could be derived, as it was done for the famous Crab pulsar (Tennant et al. 2001) and PSR J0205+6449 in the supernova remnant (SNR) 3C 58 (Slane et al. 2004). However, recent observations with *Chandra* and *XMM*-Newton showed that this is not always the case: the famous Vela pulsar ($\tau_c = 11.3$ kyr) and PSR J1119–6127 ($\tau_c$=1.6 kyr) are examples of young NSs with the bulk of the X-ray flux of a thermal origin (Pavlov et al. 2001; Gonzalez et al. 2005). Thermal emission of the NS surface is of a special interest because confronting observational data with theoretical models of the thermal radiation, presumably formed in NS atmospheres, can allow one to infer the surface temperatures, magnetic fields, and chemical composition, constrain the NS mass and radius and, eventually, understand the fundamental properties of the superdense matter in the NS interior (see Zavlin 2007a for the latest review on the theory and observations of NS thermal emission).

According to the *ATNF Pulsar Catalogue*[1] (Manchester et al. 2005), about two dozen young pulsars with ages of $\tau_c < 15$ kyr are currently known. At a distance of $d \simeq 2.5$ kpc derived from the pulsar's dispersion measure and the NE2001 galactic electron density model of Cordes & Lazio (2003), PSR J1357–6429 ($P = 166$ ms, $\tau_c = 7.3$ kyr, $\dot{E} = 3.1 \times 10^{36}$ ergs s$^{-1}$) is the third nearest object in this group (after the Vela and Crab pulsars, with $d \simeq 0.3$ and 1.7 kpc, respectively). As discussed by Camilo et al. (2004), the actual pulsar's age, $\tau$, could be related to the characteristic one as $\tau = 2\tau_c[1 - (P_0/P)^{n-1}]/[n-1]$, with a typical value of the magneto-dipole braking index $n \simeq 2$–3 (see Livingstone et al. 2006 and references therein) and a probable initial spin period of the pulsar (at its birth), $P_0 \ll P$. If true, then $\tau \lesssim 15$ kyr, still making PSR J1357–6429 a young pulsar. In addition, radio data on this pulsar collected during a 4.5-yr period (Camilo et al. 2004) revealed a strong glitch

[1] `http://www.atnf.csiro.au/research/pulsar`

of its spin period, $\Delta P/P \simeq -2.4 \times 10^{-6}$, similar to those experienced by some other young pulsars, supporting the hypothesis that PSR J1357–6429 is indeed a young NS. It is located at a distance of a few arcsecs from the SNR candidate G309.8–2.6 (Duncan et al. 1997), but there is no obvious connection between these two objects, opposite to the case of the majority of young pulsars associated with SNRs (see Manchester et al. 2002 and Camilo et al. 2004).

Alike many other young pulsars, PSR J1357–6429 has been observed in X-rays, with both *Chandra* and *XMM*-Newton. Sections 2 and 3 of this paper describe the X-ray observations of the pulsar and analysis of the collected data. The obtained results are discussed in Sec. 4.

## 2. Observations and data reduction

*XMM*-Newton observed PSR J1357–6429 on 2005 August 5 for 14.5 and 11.6 ks of effective exposures with the European Photon Imaging Cameras, EPIC-MOS and EPIC-pn (respectively). These instruments were operated in Full-Frame Window mode, covering a $\sim 25' \times 25'$ field of view. The highest time resolution of 73.4 ms achieved in the the EPIC-pn data is not sufficient for timing of a pulsar with a spin period of 166 ms. The EPIC data were reprocessed with the *XMM*-Newton Science Analysis Software (`SAS` v. 7.0.0), using the latest calibration files. Unfortunately, this *XMM*-Newton observation suffered from strong background flares. Because of that, the background level during more than 80% of the total observational span was higher by a factor of 3–6 and 5–20 than the "quiescent" rate (in the EPIC-MOS and EPIC-pn data, respectively).

Shortly after the *XMM*-Newton data had been collected, PSR J1357–6429 was observed with the *Chandra* High Resolution Camera (HRC-S) operated in Timing mode in two occasions on 2005 November 18 and 19, for 16.1 and 17.1 ks of effective exposure. After correcting time-tags of detected events for the instrumental wiring error, this mode provides the time resolution of 16 $\mu$s. The HRC-S data were reprocessed with the Chandra Interactive Analysis of Observations (`CIAO`) software (v. 3.4; `CALDB` ver.3.3.0.1), starting from the level 1 event files and applying the latest degap corrections. The level 2 event files from the two observations were combined together using the `CIAO` script `'merge_all'`, that resulted in the final data product (with a 33.2 ks exposure) used for the analysis. The pulse-invariant (PI) channels with PI$<$ 25 or PI$>$ 150 were filtered out to minimize background contamination.

The *Chandra* HRC-S data were used for a spatial and timing analysis, whereas the *XMM*-Newton EPIC data provided spectral information on X-ray emission associated with

PSR J1357–6429.

## 3. Observational results

### 3.1. Spatial analysis

Figure 1 presents a smoothed image of the $8'' \times 8''$ region around the radio position of PSR J1357–6429 derived by Camilo et al. (2004). This image reveals a point-like X-ray source surrounded by a weaker diffuse emission. The source is centered at the position R.A.= $13^{\rm h}57^{\rm m}2\overset{\rm s}{.}54$ and Dec.= $-64°29''30\overset{''}{.}0$. The difference of $0\overset{''}{.}74$ between this X-ray position and the pulsar's radio position is very close to the $1\sigma$ error in the *Chandra* HRC-S positional astrometry[2]. The diffuse-emission feature, extending toward east-north to a distance of about $2''$ from the center of the point-like source, is seen in the both HRC-S datasets and cannot be an image artifact caused by the instrument anomalies and/or background[3]. The presence of the extended emission is also apparent in Fig. 2 which shows two one-dimensional distribution of counts in rectangular apertures with a $1\overset{''}{.}84$ height and widths of either $0\overset{''}{.}13$ or $0\overset{''}{.}40$ (see bin sizes in Fig. 2) shifted along the main symmetry axis of the box plotted in Fig. 1 (the height of the apertures is parallel to the shorter side of the box): one histogram presents the distribution of detected counts, the other indicates the HRC-S point-spread function computed from a two-dimension simulation performed with the `CIAO 'mkpsf'` tool. The proximity of the X-ray and radio positions and the morphology of the extended feature strongly suggest that the detected X-ray radiation is emitted by PSR J1357–6429 and its PWN.

The elongated "tail" of the diffuse emission (within the $1\overset{''}{.}0.5 \times 1\overset{''}{.}58$ box shown in Fig. 1) contains $15.5 \pm 4.5$ background-subtracted counts, that corresponds to the averaged brightness of 0.28 counts arcsec$^{-2}$ ks$^{-1}$. Modeling the tail's emission with a power-law (PL) spectrum of a photon index $\Gamma = 1.5$ (typical for X-ray PWNe — see, e.g., Kargaltsev et al. 2007) absorbed with the hydrogen column density $n_{\rm H,21} = n_{\rm H}/(10^{21}\,{\rm cm}^{-2}) = 5.0$ (see Sec. 3.3) yields the tails's intensity $I_{\rm tail} \simeq 2.2 \times 10^{-14} d_{2.5}^2$ ergs cm$^{-2}$ s$^{-1}$arcsec$^{-2}$ ($d_{2.5} = d/[2.5\,{\rm kpc}]$) in the 0.2–10 keV range, or the luminosity $L_{\rm tail} \simeq 2.5 \times 10^{31} d_{2.5}^2$ ergs s$^{-1}$.

No large-scale signatures of a diffuse emission which could be associated with the SNR candidate G309.8–2.6 (Sec. 1) were found in the HRC data. An upper limit on the averaged surface brightness of the possible SNR emission, estimated from the $2\overset{'}{.}5$-radius circle centered

[2] `http://asc.harvard.edu/cal/ASPECT/celmon`

[3] `http://cxc.harvard.edu/proposer/POG/html/HRC.html`

at the position R.A.= $13^h56^m57\overset{s}{.}0$ and Dec.= $-64°28''00$, is 5 counts ks$^{-1}$ arcmin$^{-2}$.

### 3.2. Timing analysis

For the timing analysis, 137 counts were extracted from the $1\overset{''}{.}05$-radius circle centered at the X-ray position of PSR J1357–6429 (Sec. 3.1). Of them, 132 counts were estimated to be associated with the pulsar. The times of arrival for the extracted photons were corrected to the solar system barycenter using `CIAO 'axBary'` tool. The standard $Z_n^2$-test (e. g., Zavlin et al. 2000) was used to search for pulsations of the pulsar's X-ray flux. At the radio ephemeris obtained by Camilo et al. (2004) and extrapolated to the epoch of the *Chandra* HRC-S observations, this test results in the values of $Z_1^2 = 11.0$ and $Z_2^2 = 14.8$, that corresponds to a signal detection at a 99.6% ($3\sigma$) significance level. As the pulsar might have experienced a glitch during or shortly before the *Chandra* HRC-S observations, the $Z_n^2$ statistic was computed in a vicinity of the radio spin frequency, with the maximum values of $Z_1^2 = 12.9$ and $Z_2^2 = 15.5$ at a frequency deviating from the radio one by about 1 $\mu$Hz$\simeq 0.1/t_{\rm span}$ (where $t_{\rm span} = 94.6$ ks is the total time span of the two combined HRC-S observations). This indicates that the timing solution found by Camilo et al. (2004) and formally valid only till 2004 April (53,104 MJD) is applicable for the HRC-S data.

Figure 3 presents the pulse profile of PSR J1357–6429 extracted at the radio pulsar parameters. Because of the poor statistics, neither the shape nor the pulsed fraction, $f_{\rm p} = 57 \pm 20\%$, is well determined. One may speculate that the extracted (energy-integrated) light curve has two peaks of different widths and heights, separated by $\Delta\phi \simeq 0.4$ in phase. The only rather certain fact is that the pulsed fraction is large, implying special properties of the pulsar's emission.

### 3.3. Spectral analysis

To optimize the signal-to-noise ratio, the *XMM*-Newton EPIC-pn and MOS spectra were extracted from $20''$-radius circles centered at the pulsar position (obviously, these included the emission of the faint PWN suggested by the HRC-S data). The extraction regions contain about 75% of the source flux. The instrumental responses were generated with the `SAS 'rmfgen'` and `'arfgen'` tools (the latter accounts for the size of the extraction area). Background was evaluated from similar regions in vicinity of the pulsar position. The estimated source count rates (corrected for the finite extraction aperture) are $56 \pm 5$ and $17 \pm 2$ counts ks$^{-1}$ in the 0.3–10 keV range for EPIC-pn and EPIC-MOS, respectively. The

upper panel of Fig. 4 shows the extracted spectra.

A single PL model fits the observed spectra rather well, with $\min\chi^2_\nu = 1.17$ for $\nu = 59$ d.o.f, yielding the photon index $\Gamma = 2.1 \pm 0.4$ and $n_{\rm H,21} = 2.3 \pm 0.8$ ($1\sigma$ errors are given here and below). The derived nonthermal (isotropic) luminosity in the 0.2–10 keV range is $L_{\rm nonth} \simeq 2.1\times10^{32} d^2_{2.5}$ ergs s$^{-1}$= $6.8\times10^{-5}\dot{E}d^2_{2.5}$ (of this, about 10% belongs to the PWN). On the other hand, it is reasonable to assume that PSR J1357–6429 emits observable thermal radiation, as PSR J1119–6127 and Vela, with similar pulsar parameters, do (see Sec. 1). Adding a thermal component improves the fit, $\min\chi^2_\nu$=0.76 for $\nu$=57 d.o.f, indicating that it is required by the data at a 99.9998% ($4.8\sigma$) confidence level. The thermal component can be equally well described with both a blackbody (BB) spectrum and a NS magnetized ($B\sim10^{13}$ G) hydrogen atmosphere model[4]. However, as in many other cases, the estimates on the temperature and size of the emitting area yielded by these two models are very different(see Zavlin 2007a for details): $T^\infty_{\rm bb} = 1.7 \pm 0.2$ MK and $R^\infty_{\rm bb} = (2.5 \pm 0.5) d_{2.5}$km (redshifted values) in the BB fit, and $T_{\rm eff} = 1.0 \pm 0.1$ MK (effective temperature) for $R = 10$ km at $d_{2.5} = 1$ in the NS atmosphere fit (the NS radius and distance were fixed to reduce the correlation of fitting parameters). The corresponding bolometric luminosities are $L^\infty_{\rm bb} \simeq 3.7\times10^{32} d^2_{2.5}$ ergs s$^{-1}$ and $L_{\rm atm} \simeq 7.1\times10^{32}$ ergs s$^{-1}$ (note that $L^\infty_{\rm atm} = [1-2GM/c^2R]L_{\rm atm} \simeq 0.6L_{\rm atm}$ for the standard NS mass $M = 1.4M_\odot$ and radius $R = 10$ km). The parameters of the nonthermal component are similar, $\Gamma = 1.3\pm0.2$ and $1.1\pm0.2$, in the BB and atmosphere fits (respectively), with $L_{\rm nonth} \simeq 1.5\times10^{32} d^2_{2.5}$ ergs s$^{-1}$= $4.8\times10^{-5}\dot{E}d^2_{2.5}$. The inferred hydrogen column density (the same in the both fits), $n_{\rm H,21} = 4.9 \pm 2.0$, is somewhat larger than in the single-PL interpretation but still consistent with the standard estimate suggested by the pulsar dispersion measure DM = 127.2 cm$^{-3}$ pc, $n_{\rm H,DM}/(10^{21}\,{\rm cm}^{-2}) = {\rm DM}/(10^{20}\,{\rm cm}^{-2}) \simeq 4.0$ (assuming a 10% ionization degree of the interstellar hydrogen), and is reasonably lower than the galactic neutral hydrogen density estimated in the direction to PSR J1357–6429, $n_{\rm HI}/(10^{21}\,{\rm cm}^{-2}) \simeq 10.0$. The increase in the hydrogen column density inferred in the two-component fit explains the difference in the total X-ray luminosity measured in this and single-PL fits. The best two-component fits involving the NS atmosphere models is shown in Fig. 4.

## 4. Discussion

The first short observations of PSR J1357–6429 with *Chandra* and *XMM*-Newton have revealed rather interesting X-ray properties of this object. First of all, it is the strong

[4]Implemented as the `'nsa'` code in the XSPEC spectral fitting package.

indication of the compact tail-like PWN connected to the pulsar. The estimated efficiency with which PSR J1357–6429 powers its PWN, $L_{\rm tail}/\dot{E} \approx 0.8 \times 10^{-5}$, can be considered as "medium" among those measured for tail-like PWNe associated with other pulsars. For example, it is lower by about an order of magnitude than the efficiencies of the PWNe of the young pulsar B1757–24 (Kaspi et al. 2001) and the millisecond pulsar B1957+20 (Stappers et al. 2003; Zavlin 2007b) but larger by a factor of a few than those inferred for the Geminga's tail (Pavlov, Sanwal, & Zavlin 2006) and the Vela's southest jet (Pavlov et al. 2003). On the other hand, the derived luminosity of the tail-like X-ray feature associated with PSR J1357–6429 is about by a factor of 5–8 smaller than the nonthermal luminosity emitted by the pulsar itself, that does not match the correlation, $L_{\rm PWN} \approx 5L_{\rm nonth}$, inferred by Kargaltsev et al. (2007) for a sample of pulsars with ages $\tau_{\rm c} \simeq$ 10–30 kyr powering X-ray nebulae. Obviously, it is premature to make any certain conclusions about the properties of the possible PWN because of too scanty data available. However, despite the proper motion of PSR J1357–6429 has not been measured yet, the shape and estimated luminosity of this elongated feature suggest a feasible hypothesis that it is a pulsar jet along the pulsar's spin axis aligned with its velocity, similar to the interpretation proposed for the tail-like features of the Crab, Vela, and Geminga pulsars (Weisskopf et al. 2000; Pavlov et al. 2003; Pavlov, Sanwal, & Zavlin 2006). Future measurement of the pulsar's proper motion is important for validating this hypothesis.

The spectral data on PSR J1357–6429 show at a rather high confidence level that the bulk of the pulsar's X-ray flux is of a thermal origin. It makes this object the second youngest NS in the group of young and energetic radio pulsars with a thermal X-ray component dominating at lower photon energies ($E \lesssim 2$ keV). In addition to PSRs J1119–6127, J1357–6429 and Vela, the group also includes PSRs B1706–44 with $\tau_{\rm c} = 17.5$ kyr, J0538+2817 with the true age $\tau \simeq 30$ kyr (Kramer et al. 2003), and B2334+61 with $\tau_{\rm c} = 40.9$ kyr (see Zavlin 2007a and details and references)[5]. Similar to the situation with the thermal radiation of all other members of this group, the origin of thermal component of PSR J1357–6429 cannot be unambiguously determined from the spectral data alone. The parameters of the thermal component obtained with the BB model may be interpreted as radiation from a small hot area (polar caps) on the NS surface, although the derived radius, $R_{\rm bb}^{\infty} \simeq 2.5$ km, is much greater than the canonical polar cap estimate, $R_{\rm pc} = (2\pi R^3/cP)^{1/2} \simeq 0.3$ km. Opposite to these results, the fit with the magnetized NS atmosphere models indicate that the thermal emission originates from the entire NS surface. One could discriminate between these two interpretations invoking pulsations of the X-ray emission. In the case of PSR J1357–

[5]One more plausible candidate to this group is the putative young pulsar CXOU J061705.3+222127 powering a bright X-ray PWN near the SNR IC443.

6429, as the *Chandra* HRC-S instrument is most efficient at $E \lesssim 2$ keV, the large estimated pulsed fraction of the X-ray flux, $f_{\rm p} \gtrsim 40\%$, suggests that the thermal emission is intrinsically anisotropic, as predicted by the NS atmosphere models — otherwise the effect of strong gravitational bending of photon trajectories near the NS surface would strongly suppress the pulsations (e. g., Zavlin, Shibanov, & Pavlov 1995). This obviously contradicts the simplistic (isotropic) BB interpretation. In addition, the large pulsed fraction also indicates that the pulsar has a strong nonuniformity of the surface temperature and magnetic field. Hence, the temperature $T_{\rm eff}$ inferred from the NS atmosphere fit assuming the uniform surface should be considered as an approximate estimate on the "mean" surface temperature. The same conclusions stand for PSR J1119–6127 with a pulsed fraction $f_{\rm p} \gtrsim 60\%$ (Canzalez et al. 2005), as well as PSR 0538+2817 whose pulse profile of the thermal flux emission shows a complicate dependence on photon energy (Zavlin & Pavlov 2004).

Assuming that the characteristic ages of the five pulsars of this group are close to the true ones[6], one can compare NS cooling models with the surface temperatures estimated for these objects from fits with NS atmosphere models. Figure 5 presents cooling models with and without proton ('2p' model) superfluidity in the NS core (Yakovlev & Pethick 2004; Yakovlev et al. 2005). The superfluidity reduces the neutrino emission by suppressing the Urca processes and, hence, decelerates the NS cooling. This effect depends on NS mass, being stronger for higher masses. Comparing the estimated surface temperatures with the cooling models suggests that the interiors of these six pulsars are superfluid, and the NS masses may be in the (1.5–1.6) $M_{\odot}$ range (but note that this range would be different for another model superfluidity).

To conclude, despite the important X-ray information on PSR J1357–6429 already available, longer and dedicated observations are required to provide new data of much better quality to firmly establish the actual shape, size, and spectrum of the possible PWN, and accurately infer the X-ray spectral and temporal properties of the pulsar in a phase-resolved spectral and energy-resolved timing analysis.

The author thanks Dmitry G. Yakovlev for providing the NS cooling models. This work is supported by a NASA Fellowship Award at the NASA MSFC.

[6]This assumption should be taken with caution as, e. g., $\tau_{\rm c} \simeq 20.5\tau$ for PSR J0538+2817.

## REFERENCES

Camilo, F., Manchester, R. N., Lyne, A. G., et al. 2004, ApJ, 611, L25

Cordes, J. M., & Lazio, T. J. W. 2003, preprint (astro-ph/0301598)

Duncan, A. R., Stewart, R. T., Haynes, R. F., & Jones, K. L. 1997, MNRAS, 287, 722

Gonzalez, M. E., Kaspi, V. M., Camilo, F., Gaensler, B. M., & Pivovaroff, M. J. 2005, ApJ, 630, 489

Harding, A., & Muslimov, A. 2005, Ap&SS, 297, 63

Kargaltsev, O. Y., Pavlov, G. G., & Garmire, G. P. 2007, ApJ, in press (astro-ph/0611599)

Kaspi, V. M., Gotthelf, E. V., Gaensler, B. M., & Lyutikov, M. 2001, ApJ, 562, L163

Kramer, M., Lyne, A. G., Hobbs, G., Löhmer, O., Carr, P., Jordan, C., & Wolszczan, A. 2003, ApJ, 593, L31

Liningstone, M. A., Kaspi, V. M., Gotthelf, E. V., & Kuiper, L. 2006, ApJ, 647, 1286

Manchester, R. N., Bell, J. F., Camilo, F., et al. 2002, in ASP Conf. Ser. 271, Neutron Stars and Supernova Remnants, ed. P. O. Slane & B. M. Gaensler (San Francisco: ASP), 31

Manchester, R. N., Hobbs, G. B., Teoh, A., & Hobbs, M. 2005, AJ, 129, 1993

Pavlov, G. G., Zavlin, V. E., Sanwal, D., Burwitz, V., & Garmire, G. P. 2001, ApJ, 552, L129

Pavlov, G. G., Teter, M. A., Kargaltsev, O. Y., & Sanwal, D. 2003, ApJ, 591, 1157

Pavlov, G. G., Sanwal, D., & Zavlin, V. E. 2006, ApJ, 643, 1146

Slane, P. Helfand, D. J., van der Swaluw, E., & Murray, S. S. 2004, ApJ, 616, 403

Stappers, B. W., Gaensler, B. M., Kaspi, V. M., van der Klis, M., & Lewin, W. H. G. 2003, Science, 299, 1372

Tennant, A. F., Becker, W., Juda, M., et al. 2001, ApJ, 554, L173

Yakovlev, D. G., & Pethick, C. J. 2004, ARA&A, 42, 169

Yakovlev, D. G., Gnedin, O. Y., Gusakov, M. E., Kaminker, A. D., Levenfish, K. P., & Potekhin, A. Y. 2005, Nuc. Phys. A, 752, 590

Weisskopf, M. C., Hester, J. J., Tennant, A. F., et al. 2000, ApJ, 536, L81

Zavlin, V. E., Shibanov, Yu. A., & Pavlov, G. G. 1995, Astron. Lett., 21, 49

Zavlin, V. E., Pavlov, G. G., Sanwal, D., & Trümper, J. 2000, ApJ, 540, L25

Zavlin, V. E., & Pavlov, G. G. 2004, Mem.S.A.It., 75, 458

Zavlin, V. E. 2007a, in The 363-rd Heraeus Seminar on Neutron Stars and Pulsars, Springer Lecture Notes, in press (astro-ph/0702426)

Zavlin, V. E. 2007b, Ap&SS, in press (astro-ph/astro-ps/0608210)

Zhang, L., & Jiang, Z. J. 2006, A&A, 454, 537

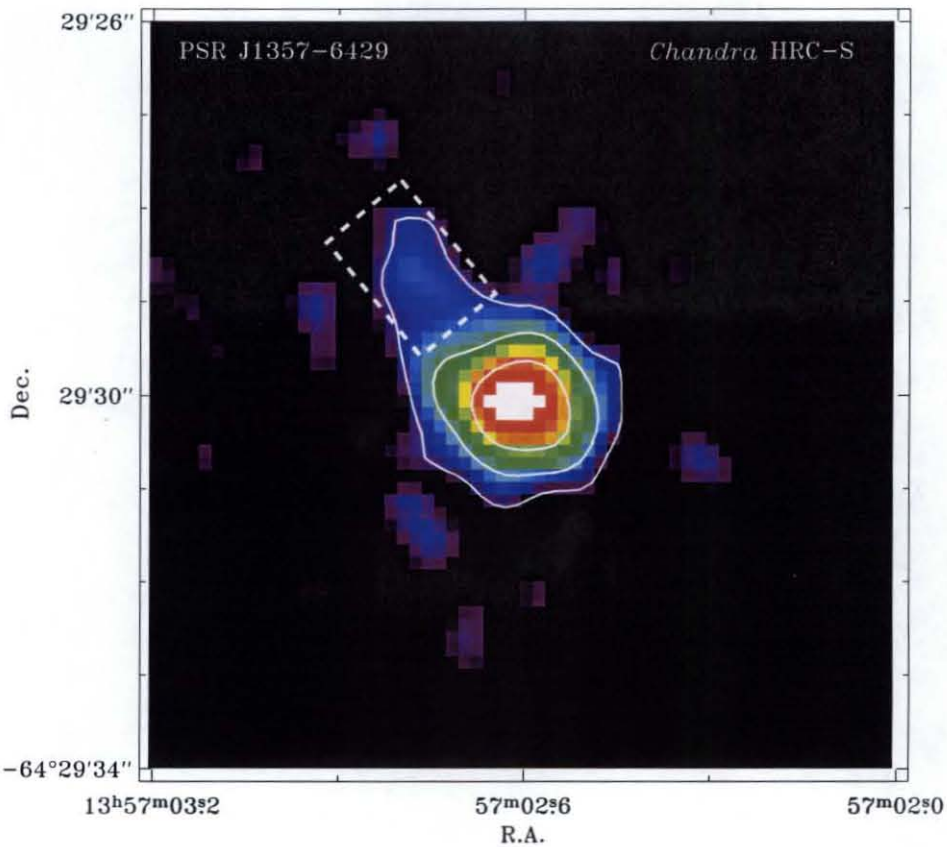


Fig. 1.— *Chandra* HRC-S 8″ × 8″ image (smoothed with a 0.″4 FWHM Gaussian) showing PSR J1357–6429 surrounded by an extended structure elongated in the east-north direction (indicated by the white-dashed box of a 1″ × 1.″5 size). White (solid) contours correspond to intensity values of 0.17, 0.55, and 1.74 counts arcsec$^{-2}$ ks$^{-1}$.

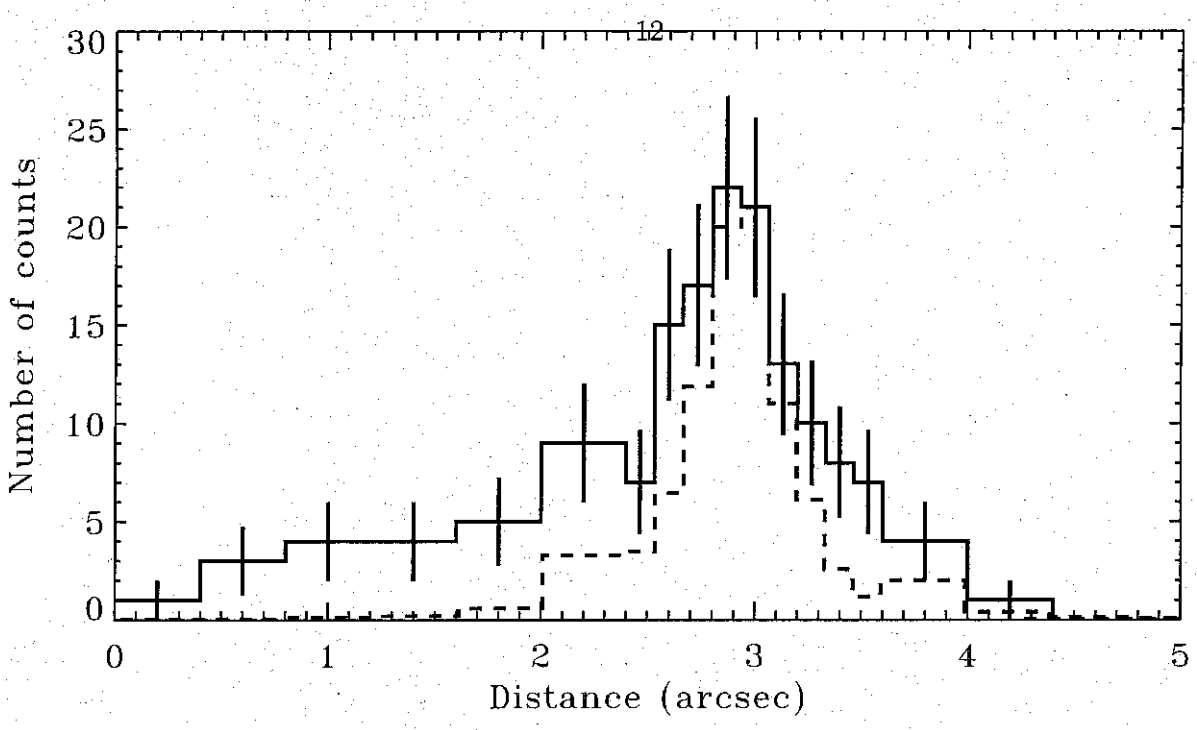


Fig. 2.— Distribution of counts detected with the *Chandra* HRC-S instrument (solid histogram) in rectangular apertures with a 1.″84 height and varying widths (0.″13 or 0.″40) shifted along the main symmetry axis of the box shown in Fig. 1. The dashed histogram shows the HRC-S point-spread function computed for the same apertures.

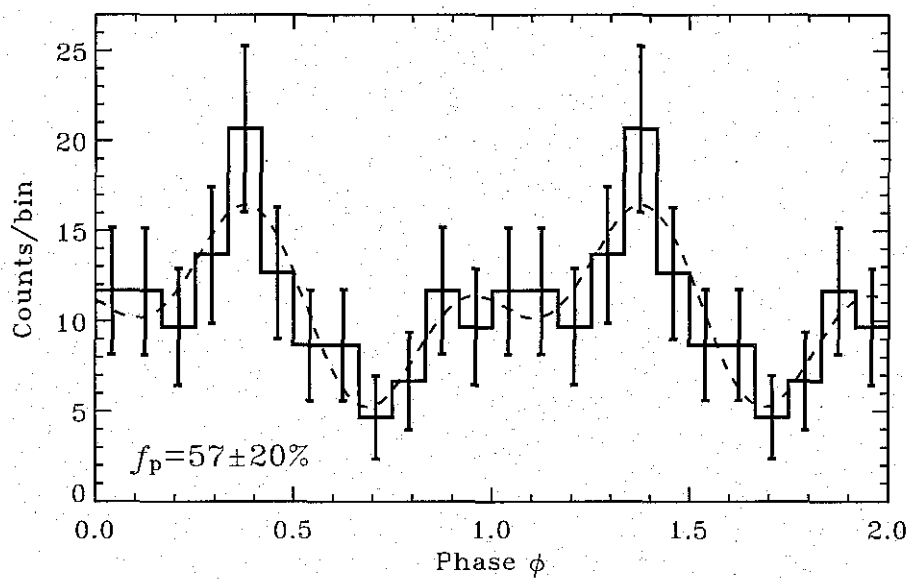


Fig. 3.— Pulse profile of PSR J1357–6429 extracted from the *Chandra* HRC-S data and fitted with a two-harmonic model (dashes). The estimated pulsed fraction, $f_p$, is indicated.

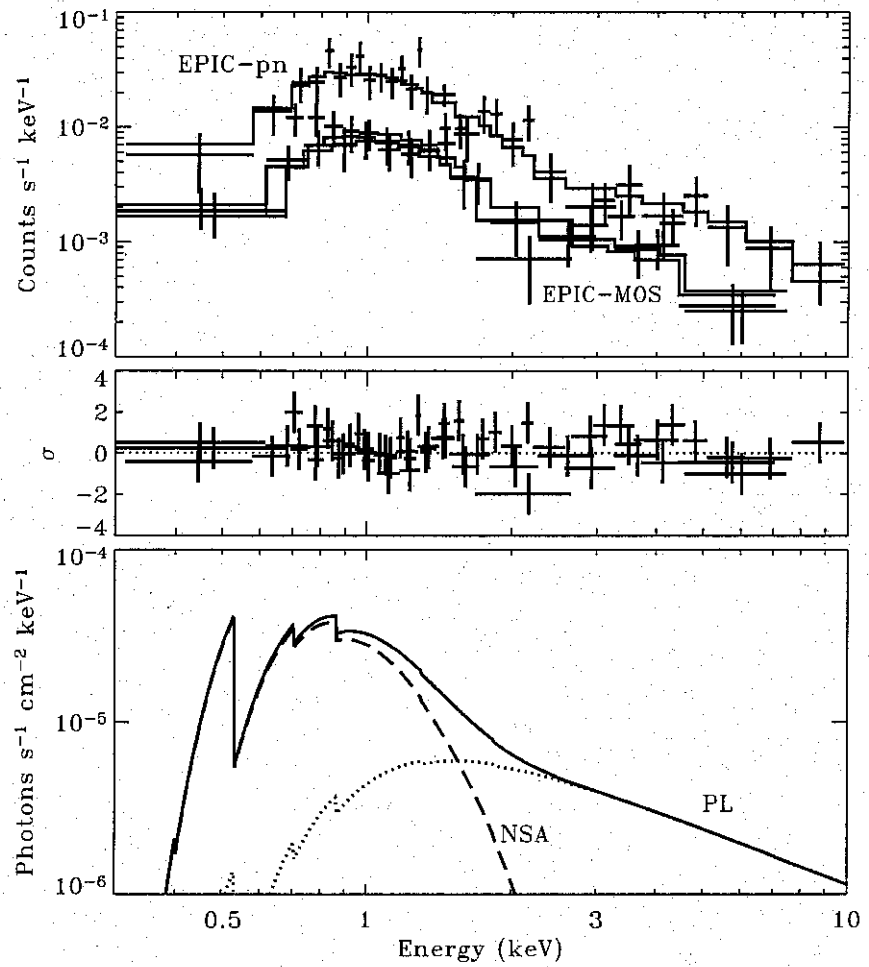


Fig. 4.— Spectra of PSR J1357–6429 detected with three *XMM*-Newton EPIC instruments and fitted with a two-component, NS atmosphere (NSA) plus power law (PL), model.

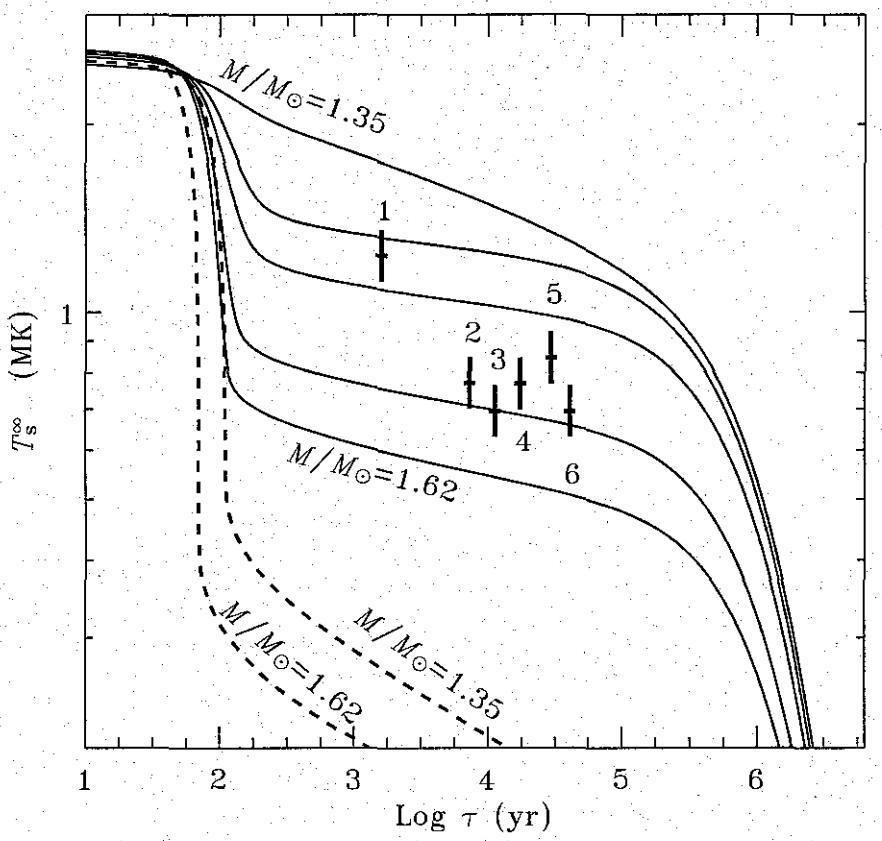


Fig. 5.— NS cooling models (Yakovlev & Pethick 2004) with the so-called '2p' proton superfluidity (solid curves) for NS masses $M/M_\odot$ = 1.35, 1.49, 1.56, 160, and 1.62 (from the upper curve to the lower one) and without the superfluidity (two dashed curves for $M/M_\odot$ = 1.35 and 1.62). The crosses indicate the pulsars: J1119–6127 (1), J1357–6429 (2), Vela (3), B1706-44 (4), J0538+2817 (5), and B2334+61 (6). The redshifted surface temperature is estimated as $T_s^\infty = [1 - 2GM/c^2R]^{1/2} T_{\rm eff} = 0.77 T_{\rm eff}$ (for $M/M_\odot$ = 1.4 and $R$ = 10 km), where $T_{\rm eff}$ is the effective (mean) temperature of the NS surface obtained with use of NS atmosphere models (see Sec. 3.3 and Zavlin 2007a for details).